Journal of Materials Chemistry B

Accepted Manuscript

ROYAL SOCIETY OF CHEMISTRY

www.rsc.org/materialsB

Journal of Materials Chemistry B

ARTICLE

Received 00th January 20xx,
Accepted 00th January 20xx

DOI: 10.1039/x0xx00000x

www.rsc.org/MaterialsB

[a] *Centre de recherche en organogénèse expérimentale de l'Université Laval / LOEX, Québec, Qc, Canada*
[b] *Division of Regenerative Medicine, CHU de Québec – Université Laval Research Center, Québec, Qc, Canada*
[c] *Department of Surgery, Faculty of Medicine, Université Laval, Québec, Qc, Canada*
* Corresponding author
‡ Address: CMDGT/LOEX, Aile-R, CRCHU de Québec-Hôpital Enfant-Jésus, 1401, 18e Rue, Québec, Qc, Canada, G1J 1Z4. Email: julie.fradette@chg.ulaval.ca; Tel: 1-418-990-8255 Ext.61713; Fax: 1-418-990-8248
† Supplementary Information (ESI) available: See DOI: 10.1039/x0xx00000x

ARTICLE Journal of Materials Chemistry B

Impact of TNF and IL-1β on capillary networks within engineered human adipose tissues†

Maryse Proulx,[ab] Meryem Safoine,[ab] Dominique Mayrand,[ab] Kim Aubin,[ab] Amandine Maux,[ab] and Julie Fradette*[abc‡]

Inflammation is a normal phase of the wound healing process likely to occur following tissue transplantation. For reconstructive surgery purposes, engineered adipose tissues represent a promising alternative to autologous fat grafts. It is therefore important to study the impact of an inflammatory microenvironment on the cellular functions of the different cell types comprised within matrix-rich reconstructed tissues. In this study, human reconstructed adipose tissues (hrATs) featuring a preformed capillary network formed by microvascular endothelial cells (hMVECs) were produced from adipose-derived stem/stromal cells (ASCs) by the self-assembly approach of tissue engineering. We hypothesized that a prolonged inflammatory context, mediated by tumor necrosis factor (TNF) and interleukin-1β (IL-1β), would impact hrATs secretory profile and mediate detrimental effects on the microvascular network *in vitro*. Analysis of conditioned media established tissue responsiveness through increased secretion of monocyte chemoattractant protein-1 (up to 23 fold), interleukin-6 (up to 69 fold) and angiopoietin-1 (up to 2.7 fold) after 3 and 6 days of cytokine exposure, along with a significant reduction in adiponectin secretion. Imaging of the preformed capillary network within the hrATs revealed increased disorganization in presence of TNF/IL-1β, featuring a less extended and less ramified network with apoptotic hMVECs in the remaining capillary structures. These results indicate that a prolonged inflammatory context can be deleterious for the capillary network featured by *in vitro* engineered tissues. Strategies aiming at preserving the integrity of the vascular network will help develop substitutes that are better suited to face inflammatory conditions upon grafting.

Introduction

Adipose tissue (AT) is a highly vascularized organ containing many capillaries surrounding lipid-filled adipocytes,[1] in addition to multipotent adipose-derived stem cells (ASCs) present within the stroma.[2] The close spatial localization of the vascular compartment and adipocytes is indicative of the relation between adipogenesis and angiogenesis, which are intimately linked during development and even into adulthood.[3] AT's wide range of cellular functions has been underestimated for a long time, but AT is now recognized as a key secretory organ responsible for the production of hormones, chemokines, growth factors and cytokines mediating autocrine, paracrine and endocrine responses.[4-7] For instance, AT secretes the anti-inflammatory hormone adiponectin,[8] the pro-inflammatory interleukin-6 (IL-6)[9] and the chemokine monocyte chemoattractant protein-1 (MCP-1)[10] implicated in the recruitment of monocytes at a site of inflammation. AT also produces the blood vessel stabilizing factor angiopoietin-1 (Ang-1) and its natural antagonist angiopoietin-2 (Ang-2).[11-13] The matrix metalloproteinases (MMPs) MMP-2 and MMP-9, which are also expressed by AT, contribute to matrix remodeling and angiogenesis regulation.[14-16] AT therefore represents a dynamic tissue undergoing expansion and remodeling in response to various intrinsic and external stimuli.

AT grafts are needed for reconstructive surgery purposes to treat patients presenting soft tissue lesions resulting from tumor resections, accidents, deep burns and also congenital defects. *In vitro* engineering of AT substitutes is considered as a promising alternative to native fat grafting.[17] To ensure survival and long-term function of AT substitutes, a rapid and timely vascularization from the host is required, providing oxygen and nutrients.[18, 19] Among other strategies, the integration of a vascular component to *in vitro* engineered substitutes has been proposed as a way to favor inosculation between the host and the *in vitro* preformed capillary network.[20] Upon grafting *in vivo*, engineered AT substitutes can face an inflammatory microenvironment resulting from tissue injury at the site of implantation.[21] In fact, tissue damage induces the recruitment of neutrophils and monocytes that will differentiate into macrophages and secrete important amounts of pro-inflammatory cytokines such as tumor necrosis factor (TNF) and interleukin-1β (IL-1β).[21] A prolonged or deregulated pro-inflammatory environment can be detrimental to the implanted grafts.[21, 22]

Many studies established that ASCs and adipocytes within AT are responsive to pro-inflammatory cytokines. Indeed, TNF and IL-1β are known to inhibit adipogenic differentiation, induce lipolysis, and modify lipid metabolism in addition to secretory functions.[23-32] Our previous work showed that engineered adipose sheets produced according to the self-assembly method are responsive to the pro-inflammatory stimulus TNF. Indeed, the expression of metabolism-associated genes (*SLC2A4*, *FASN*, *LIPE*) and also of members and targets of the NF-κB pathway was modulated following exposure to this cytokine.[33] Importantly, the impact of pro-inflammatory cytokines on endothelial cells and on the vascular network of AT is less characterized.[34-36] Even though microcirculation is recognized as an important target of inflammation, opposing effects have been reported depending on endothelial cell origin, experimental context and pro-inflammatory cytokine

concentrations. Indeed, not only tube formation inhibition and induction of apoptosis were observed, but also stimulation of angiogenic processes.[37-44] It is therefore important to study the impact of inflammatory stimuli on capillary networks specifically within the adipose microenvironment when trying to predict the fate of AT substitutes as graft material.

In this study, we produced human reconstructed adipose tissues (hrATs) containing a preformed capillary network following the incorporation of microvascular endothelial cells (hMVECs) during tissue production. The resulting three-dimensional (3D) substitutes (hrATs+hMVECs) hence contained adipocytes and capillary-like structures surrounded by undifferentiated ASCs embedded in a human neosynthesized extracellular matrix (ECM), which deposition is stimulated by ascorbic acid. We took advantage of the stability of our *in vitro* model[33, 45] to study the impact of a long-term pro-inflammatory cytokine exposure (6 days *in vitro*). We hypothesized that TNF and IL-1β would recreate an inflammatory context impacting on the secretory profile of cells within hrATs+hMVECs, in addition to deleterious effects on the established capillary network. First, we determined the modulation of the secreted levels of adiponectin, MCP-1, IL-6, Ang-1, Ang-2, MMP-2 and MMP-9 following a chronic exposure to TNF and IL-1β, alone or in combination. Then, we carefully detailed the impact of TNF and/or IL-1β on the total length of the capillary network, on the percentage of branched structures and on the induction of apoptosis within this microvascular network. Our results establish that prolonged inflammation markedly impact the release of secreted proteins (cytokines, growth factors, MMPs) as well as the integrity of the capillary network featured by *in vitro* engineered AT substitutes.

Materials and methods

Cell isolation

All human cell populations were obtained after written informed consent of donors. Protocols were approved by the Ethics Committee of the CHU de Québec Research Center. Human ASCs were isolated using collagenase digestion as described earlier[46] from subcutaneous white adipose tissue of 4 female donors (mean age: 37.8 ± 4.6, mean body mass index: 26.3 ± 2.8) undergoing lipoaspiration procedures (Table S1, ESI†). ASCs were amplified in DH medium (1:1 Dulbecco's Modified Eagle Medium (DMEM): Ham's F12 medium (H), Life Technologies, Burlington, ON, Canada) containing 10% fetal calf serum (FCS) (HyClone, Thermo Scientific, Logan, UT, USA) and antibiotics [100 U ml^{-1} penicillin (Sigma, Oakville, ON, Canada) and 25 µg ml^{-1} gentamicin (Schering-Plough Canada Inc / Merck, Scarborough, ON, Canada)] at a density of 6-8 x 10^4 cells cm^{-2} in NUNC flasks (Thermo Scientific, Ottawa, ON, Canada). They were batch frozen at passage (P) 0 and used at P3-4 for tissue reconstruction. hMVECS were extracted from the dermis of a 59-year-old female donor after an overnight thermolysin incubation as described previously.[45] hMVECS were amplified in endothelial cell medium EGM-2MV BulletKit (Lonza, Walkersville, MD, USA) supplemented with 100 U ml^{-1} penicillin and 25 µg ml^{-1} gentamicin instead of the GA-1000 provided by the manufacturer. hMVECs were seeded at a density of 9 x 10^3 – 1 x 10^4 cells cm^{-2} on gelatin-coated (Fisher Scientific, Ottawa, ON, Canada) T75 flasks (BD Falcon, BD Biosciences, Mississauga, ON, Canada) and were seeded at P7 on human reconstructed adipose sheets or used for gene expression studies. Cells were cultured in a 37 °C incubator with 8% CO_2 humidified atmosphere.

Production of reconstructed adipose sheets and tissues

ASCs in P0 were thawed and amplified in DH medium containing 10% FCS and antibiotics (see Cell isolation section) at a density of 6.4-8.0 x 10^3 cells cm^{-2} for 2-3 passages. For sheet and tissue reconstruction using the self-assembly approach,[46, 47] ASCs were seeded in NUNC 6-well plates (Thermo Scientific) at a density of 1.64 x 10^4 cells cm^{-2} in the amplification medium supplemented with 50 µg ml^{-1} (250 µM) ascorbic acid (Sigma) prepared fresh at each medium change every 2-3 days during the entire period of tissue reconstruction. Each well contained a paper-filter anchorage device (Whatman, GE Healthcare, Ottawa, ON, Canada) to allow easy manipulation of the sheets. After 6-7 days of culture, cells were incubated with an adipogenic induction cocktail [DH medium containing 3% FCS, 100 nM insulin (Sigma), 0.2 nM triiodothyronine (T3) (Sigma), 1 µM dexamethasone (Sigma), 0.25 mM 3-isobutyl-1-methylxanthine (IBMX) (Sigma), 1 µM rosiglitazone (Cayman Chemical, Ann Arbor, MI, USA) and antibiotics] for 3 days. Then, the induction cocktail was replaced with an adipocyte maintenance medium (DH medium, 10% FCS, 100 nM insulin, 0.2 nM T3, 1 µM dexamethasone and antibiotics). At day 21-26 of culture, hMVECs were seeded on the formed adipose sheets at a density of 1.2 x 10^4 cells cm^{-2} in 1:1 adipocyte maintenance medium: EGM-2MV medium (Fig. 1). In some instances, hMVECs were first incubated with the Vybrant Dil cell-labelling solution (5 µM, Thermo Fisher) before seeding on adipose sheets to allow endothelial cell tracking. Adipose sheets not seeded with hMVECs were cultured in the same culture medium. At day 28-36 of culture, 2-sheet thick hrATs+hMVECs were produced by the superposition of one adipose cell sheet seeded with hMVECs (bottom) and one adipose cell sheet without hMVECs (top) (Fig. 1). Alternatively, two adipose sheets without hMVECs were also superposed to obtain hrATs-hMVECs as a reference group (ASCs #1 & ASCs #2). Both types of tissues were incubated in adipocyte maintenance medium for 4 days to allow hMVECs reorganization into capillary-like networks before studying the impact of inflammation (Fig. 1). Some adipose sheets (ASCs #3 & ASCs #4) were kept in culture up to 35 days (28 days of differentiation) without hMVECs nor EGM-2MV and were used for gene expression studies.

Exposure of hrATs to inflammatory cytokines

Lyophilized recombinant human TNF (EMD Millipore (Merck) / Cedarlane, Burlington, ON, Canada) was reconstituted in apyrogen water, aliquoted and stored at -20 °C as stock solution. Lyophilized recombinant human IL-1β (Fitzgerald Industries International / Cedarlane) was reconstituted in apyrogen water, further diluted in a 0.1% human serum albumin (MP Biomedicals, Solon, OH, USA) solution, aliquoted and stored at -20 °C as stock solution. At the time of incubation with tissues, cytokines were further diluted in medium and added to the cultures.

hrATs+hMVECs and hrATs-hMVECs were kept in individual 60 mm petri dishes (Fisher Scientific) and were installed on a rocker platform (Low profile rocker, Stovall Life Science, Greensboro, NC, USA) at 22 RPM with a 10° angle slope from day -1 to day 6 of cytokine treatment (Fig. 1). Daily medium changes were performed with adipocyte maintenance medium devoid of dexamethasone from day -1 to day 5. From day 0 (day 33-41 of culture) to day 6, hrATs+hMVECs and their counterparts without hMVECs were incubated with 10 ng ml^{-1} TNF, 10 ng ml^{-1} IL-1β or the combination of both (Fig. 1). Cytokines were supplemented daily with medium change. Control tissues were incubated with the appropriate vehicule solution without cytokines. The 10 ng ml^{-1} concentration was selected based on a wide number of studies reporting the impact of TNF and IL-1β on adipocyte's metabolic functions, during short- and longer term *in vitro* studies.[28-30, 48]

Quantitative real time PCR

Adipose sheets featuring adipocytes differentiated for 28 days and cultured for a total of 35 days without hMVECs nor EGM-2MV (ASCs #3 & ASCs #4, n = 3 sheets per donor) and hMVECs at P7 cultured as monolayer on gelatin-coated flasks in EGM-2MV media (n = 3) were rinsed in phosphate buffered saline (PBS), flash frozen in liquid nitrogen and conserved at -80 °C until analysis. Samples were homogenized in Qiazol buffer (Qiagen, Germantown, MD, USA) and total RNA was extracted using the RNeasy mini kit on-column DNase (Qiagen, Hilden, Germany) treatment. Quantity of total RNA was measured using a NanoDrop ND-1000 Spectrophotometer (NanoDrop Technologies, Wilmington, DE, USA) and total RNA quality was assayed on an Agilent BioAnalyzer 2100 (Agilent Technologies, Santa Clara, CA, USA). First-strand cDNA synthesis was accomplished using 1.5–5 µg of isolated RNA in a reaction containing 200 U of Superscript III Rnase H-RT (Invitrogen Life Technologies), 300 ng of oligo-dT_{18}, 50 ng of random hexamers, 50 mM Tris-HCl pH 8.3, 75 mM KCl, 3 mM $MgCl_2$, 500 µM deoxynucleotides triphosphate, 5 mM dithiothreitol, and 40 U of Protector RNase inhibitor (Roche Diagnostics, Indianapolis, IN, USA) in a final volume of 50 µl. The reaction was incubated at 25 °C for 10 min, then at 50 °C for 1 h. Subsequently, cDNA was purified using a PCR purification kit (Qiagen).

Oligoprimer pairs were designed by GeneTool 2.0 software (Biotools Inc, Edmonton, AB, Canada) and their specificity was verified by BLAST® in the GenBank database. The synthesis was performed by IDT (Integrated DNA Technology, Coralville, IA, USA) (Table S2, ESI[†]). cDNA corresponding to 20 ng of total RNA was used to perform fluorescent-based Realtime PCR quantification using the LightCycler 480 (Roche Diagnostics, Mannheim, Germany). Reagent LightCycler 480 SYBRGreen I Master (Roche Diagnostics, Indianapolis, IN, USA) was used as described by the manufacturer with 2% DMSO. The conditions for PCR reactions were: 45 cycles, denaturation at 95 °C for 10 sec, annealing at 57–62 °C for 10 sec, elongation at 72 °C for 14 sec and then 74 °C for 5 sec (reading). A melting curve profile was used to assess non-specific signal. Calculation of the number of copies of each mRNA was performed according to Luu-The *et al.*, using a second derivative method and a standard curve of Cp versus logarithm of the quantity.[49] The standard curve was established using known amounts of purified PCR products (10, 10^2, 10^3, 10^4, 10^5 and 10^6 copies) and a LightCycler 480 v1.5 program provided by the manufacturer (Roche Diagnostics). PCR amplification efficiency was verified. Quantitative Real-Time PCR measurements were performed by the CHU de Québec Research Center (CHUL) Gene Expression Platform, Québec, Canada, as described earlier[33], and were compliant with MIQE guidelines.[50, 51]

Histological analyses

Samples of hrATs+hMVECs and hrATs-hMVECs from the different experimental groups treated for 6 days were fixed for 24 h in a 3.7% buffered formalin solution and were embedded in paraffin for histological analysis. Masson's trichrome staining was performed on 5 µm-thick tissue cross-sections to highlight the extracellular matrix (blue) and the cells (pink). Two samples were photographed (2 brightfield images per sample) for each tissue (n = 2-3 tissues per condition, ASCs #2) using an Axio Imager.M2 microscope equipped with an AxioCam ICc1 camera, an EC Plan-Neofluar 10x/0.3 objective and the AxioVision software v4.8.2.0 (Zeiss, Toronto, ON, Canada). Thickness measurements were performed using the ImageJ software version 1.48r (Wayne Rasband, National Institutes of Health, Bethesda, MD, USA). Three measurements were performed on each picture for a total of 12 measurements for each tissue.

Secretion profile analysis

Media conditioned for 24 h by the tissues were collected at day 3 (ASCs #1 & ASCs #2, n = 3-4 tissues per condition) and day 6 (ASCs #2, n = 3 tissues per condition) of incubation with pro-inflammatory cytokines and were stored at -80 °C until analysis. Specific ELISA assays (Duoset®, Bio-Techne, Minneapolis, MN, USA) were performed according to the manufacturer's instructions to quantify the secreted levels of adiponectin, MCP-1, IL-6, Ang-1, Ang-2, MMP-2 and MMP-9 in conditioned media. All molecules were also quantified in the control media incubated for 24 h without the tissues. Results are expressed as pg ml^{-1} (adiponectin, Ang-1, Ang-2, MMP-9) or ng ml^{-1} (MCP-1, IL-6, MMP-2) per tissue construct. Baseline levels were subtracted if detected in the tissue-free controls

(Ang-1) except for Ang-2 for which baseline levels for each experiment are indicated.

Microvascular network characterization

Formalin-fixed hrATs+hMVECs samples incubated or not with the cytokines for 0, 3 or 6 days were used for network analysis. Immunolabelings for the endothelial cell marker CD31 and the basement membrane component laminin were performed on clarified whole-mount samples of approximately 4-9 mm^2 as described previously.[45, 52] A 1:3 solution containing 30% hydrogen peroxide: Dent's fixative was used after permeabilization in Dent's fixative alone. Nuclei were counterstained with Hoechst 33258 (0.5 µg ml^{-1}, Sigma) during the incubation with secondary antibodies.

These whole-mount labeled hrATs+hMVECs were imaged using a LSM 700 confocal microscope with a Plan-Apochromat 20x/0.8 objective and Zen 2010 software (Zeiss). Full thickness mosaic images of 928.39 µm x 928.39 µm were acquired for 2 samples of each tissue for a total analyzed surface of 1.72 mm^2. Two-dimensional (2D) renderings of the confocal images were performed using the Maximum Intensity Projection method for visualization purposes. Three-dimensional isosurface reconstructions of the capillary network of hrATs+hMVECs were obtained using the Surfaces function of the Surpass view of Imaris software (Version 7.0.0, Bitplane, Concord, MA, USA). Rounded structures under 4 500 um^3 were excluded by applying a volume filter to eliminate isolated cells and debris.

Total network length was calculated from the full thickness confocal images using the Distance tool of the Slice view of Imaris software to calculate the length of every CD31-positive segment. Data are expressed as total network length per mm^2 of imaged tissue (Day 3, ASCs #1, n = 3-4 tissues per condition; Day 6, ASCs #2, n = 3 tissues per condition). Branching points were also calculated manually from the capillary network 3D isosurface reconstructions and are expressed as the percentage of branched capillary structures.

Using Imaris software, structures were defined as an independent CD31-positive capillary or a group of interconnected capillaries. Each structure was independent and devoid of connection with one another. We defined capillary segments as subsections joined to one another through a branching point and also as isolated unbranched capillaries. Branching points were defined as the junction at which capillary segments meet and connect.

Immunolabelings for the endothelial cell marker CD31 were also performed on unpermeabilized and unclarified 3.7% formalin-fixed hrATs+hMVECs to revel the capillary-like network. After immunostaining, samples were washed in PBS and were incubated with Nile Red (200 ng ml^{-1}, Molecular Probes) for 60 min at room temperature (RT) to confirm the presence of lipid-filled adipocytes. Samples were then rinsed once in PBS and were mounted between coverslips in standard mounting medium.

Apoptotic cell detection

Quantification of apoptosis within the capillary networks was performed on hrATs+hMVECs after 3 days of cytokine exposure. Using confocal images from whole-mount tissues immunolabeled for CD31, laminin and counterstained with Hoechst 33258 as described in the «Network analysis» section, the number of apoptotic Hoechst labeled-nuclear fragments were counted manually for a mosaic image of 0.86 mm^2 (928.38 µm x 928.38 µm) and were reported per number of CD31 segment (Day 3, ASCs #1, n = 3 tissues per condition). The number of segments was determined manually from the isosurface reconstructions.

Double immunostainings for active caspase-3 and CD31 were also performed on formalin-fixed clarified whole-mount hrAT+hMVECs samples exposed to cytokines for 3 days. After permeabilization, samples were blocked in PBS containing 1% bovine serum albumin (BSA, Bio Basic Canada, Markham, ON, Canada) for 30 min at RT and were incubated at 4 °C for 48 h with a rabbit anti-active caspase-3 antibody (5 µg ml^{-1}, BD) and a sheep anti-human CD31 antibody (2 µg ml^{-1}, Bio-Techne) in a 1% BSA solution. Isotypic controls were also performed on some samples using normal rabbit (Bio-Techne) and sheep (EMD Millipore/Merck) IgGs as described above. After 3 washes with PBS, tissue samples were incubated for 48 h at 4°C with a AlexaFluor 488-conjugated donkey anti-sheep IgG (H+L) antibody and a Alexa Fluor 594-conjugated chicken anti-rabbit IgG (H+L) antibody (Molecular Probes) in a 1% BSA solution for secondary detection. Nuclei were counterstained with Hoechst 33258. After 3 washes with PBS, tissues were dehydrated in methanol series and clarified in methyl salicylate series. Three full thickness confocal images of 319.8 µm x 319.8 µm were taken for each tissue (0.31 mm^2 surface). The percentage of active caspase-3-positive CD31-positive segments was determined following manual counting (n = 3-5 tissues per condition, ASCs #1).

Statistical analyses

Data are presented as mean ± SD. When appropriate, one-way ANOVA with Dunnett's post test were performed as well as unpaired *t* tests with Welch's correction using GraphPad Prism software version 6.0 (GraphPad Software, La Jolla, CA, USA). One-way ANOVA with Dunnett's post test were performed to compare the results obtained after incubation in each cytokine condition to the control condition. Unpaired *t* tests with Welch's correction were performed to compare hrATs+hMVECs and hrATs-hMVECs within a given condition. Values of $p < 0.05$ were considered significant. * or # $p < 0.05$, ** or ## $p < 0.01$, *** or ### $p < 0.001$, **** or #### $p < 0.0001$. Symbols (* versus #) were used to indicate statistical significance in comparison to the control condition on graphs showing side by side results for hrATs produced from different cell populations (* ASCs #1; # ASCs #2). In order to perform

statistical significance analysis for MMP-9 secretion for ASCs #1, the detection limit value of the ELISA kit for the control condition value was used since MMP-9 levels were below the detection limit.

Results

ASCs as building blocks for the engineering of matrix-rich microvascularized adipose substitutes

Using the self-assembly approach of tissue engineering, hrATs+hMVECs were produced *in vitro* from human ASCs that were induced towards adipogenic differentiation while stimulated for enhanced ECM assembly/deposition with ascorbic acid in culture. Combined with the incorporation of hMVECs during tissue production (Fig. 1), the resulting tissues hence contain mature adipocytes (26-35 days of *in vitro* differentiation at day 0 of treatment), remaining undifferentiated ASCs and a microvascular network surrounded by human neosynthesized matrix. Masson's trichrome staining of histological cross-sections highlights the presence of adipocytes (void spaces) surrounded by a collagen-rich ECM (in blue, Fig. 2A-D). As evidenced on these transverse tissue sections, hrATs+hMVECs incubated with 10 ng ml^{-1} TNF (Fig. 2B), 10 ng ml^{-1} IL-1β (Fig. 2C) or the combination of both (Fig. 2D) featured increased tissue thickness (Fig. 2B, C) or matrix remodeling (Fig. 2D) after 6 days of incubation with the cytokines. In fact, thickness determination indicated that IL-1β alone mediated the maximal mean effect with a 1.6 fold increase ($p < 0.01$) when compared to the control condition (Fig. 2E). Similar observations were obtained for hrATs-hMVECs and no significant thickness differences were measured between hrATs+hMVECs and hrATs-hMVECs (Fig. 2E).

Quantitative RT-PCR performed on adipose sheets and hMVECs demonstrated the gene expression of *TNFRSF1A*, *TNFRSF1B*, *IL1R1*, *IL1R2* and *IL1RAP* coding for the TNF and IL-1β receptors and the interleukin-1 receptor accessory protein were also expressed (Table S3, ESI†).

The matrix-rich 3D microenvironment of hrATs is highly conducive to hMVECs adhesion, proliferation, migration and tubule formation, resulting into well-defined capillary-like networks.[45] Confocal microscopy images of the tissues (Fig. 2F-H) after Nile Red staining best revealed the presence of numerous adipocytes (Fig. 2F, H) as well as the spatial relationship with the CD31-expressing capillary-like network (Fig. 2G, H).

A pro-inflammatory microenvironment modulates the cellular functions of microvascularized hrATs

hrATs+hMVECs are functionally active tissues containing cells that secrete many potent bioactive molecules such as the adipokine adiponectin as well as chemokines, cytokines and growth factors such as MCP-1, IL-6 and Ang-1 (Fig. 3, control groups). The modulation of the secretion profile of hrATs+hMVECs was analyzed for these molecules using ELISA assays following a shorter (3 days, Fig. 3A) and longer (6 days, Fig. 3B) exposure to pro-inflammatory cytokines. Significant differences were determined for the secretion levels of all four molecules, for each cytokine-exposed conditions and at both time-points. In particular, while a significant decrease in adiponectin secretion was observed, robust increases in MCP-1 and IL-6 secretion levels were measured. In detail, a 3.3-fold reduction (ASCs #1) and even a decrease below the detection level (ASCs #2) were observed for adiponectin secretion after 3 days of exposure to combined TNF/IL-1 β (Fig. 3A). At the same time-point, increased levels (up to 23 fold) of MCP-1 were measured along with an increase of the pro-inflammatory cytokine IL-6 (up to 69 fold). Finally, Ang-1 secretion levels were modulated up to 2.7 fold for the combined TNF/IL-1β condition. Similar trends were observed after 6 days of exposition to pro-inflammatory cytokines (Fig. 3B).

Chronic exposure to TNF/IL-1 β leads to microvascular network disorganization and endothelial cell-apoptosis induction

Importantly, the engineered hrATs+hMVECs allowed us to determine the impact of TNF and IL-1β on hMVECs capillary networks *in vitro*. We took advantage of confocal imaging protocols to analyze large surface areas of hrATs+hMVECs samples (Fig. 4A-C) immunostained for the ECM component laminin (Fig. 4A, C, green) composing the basement membranes of adipocytes and capillaries, and for the endothelial cell marker CD31 (Fig. 4B, C, red). Three-dimensional isosurface renderings of the CD31-positive capillary network were produced at day 0 (Fig. 4D), day 3 (Fig. 4E-H) and day 6 of the indicated cytokine treatment (Fig. 4I-L), revealing drastic effects, especially for the combined cytokine condition. Indeed, the incubation of hrATs+hMVECs with the combination of TNF and IL-1β for 3 and 6 days revealed a 3.2 fold significant decrease in their total network length per mm^2 of tissue surface when compared to the control condition (Fig. 4M). A 2.3 fold decrease (non-significant) was also observed for the IL-1β only treatment after 6 days. The complexity of the capillary network of hrATs+hMVECs was also affected by the pro-inflammatory cytokines (Fig. 4N). In particular, a much lower percentage of branched capillary structures was observed after 3 and 6 days, especially in the presence of combined TNF/IL-1β (1.7 and 3.1 fold, respectively). In parallel, the secretion profile of Ang-2 was evaluated (Fig. 4O). At both time-points and for all cytokine-treated groups, secreted levels of Ang-2 were significantly reduced.

In order to gain insights into putative mechanisms mediating these effects on hMVECs forming the capillary network within engineered adipose tissues, the induction of apoptosis was assessed at day 3 of cytokine exposure. First, the presence of chromatin condensation and nuclear fragmentation was examined in CD31-positive hMVECs cells forming the capillary networks (Fig. 5A-G). For the mock-treated control condition (Fig. 5A-C), most capillaries contained few to none condensed and fragmented Hoechst-positive nuclear fragments (Fig. 5B,

C, arrows), associated with natural remodeling of capillary networks. Cytokine-exposed capillary networks contained more apoptotic nuclear fragments than the control condition. In fact, exposure to the combination of TNF and IL-1β (Fig. 5D-F), revealed the highest occurrence of apoptotic nuclei (Fig. 5E, F), as supported by the quantification of the number Hoechst-positive condensed nuclear fragments per CD31 segment reaching 5.8 fragments per segment compared to 0.76 fragment per segment for the control condition, a 7.7 fold increase (Fig. 5G).

These results were also supported by the detection of active caspase-3 in the capillary network after cytokine supplementation at the same time-point (Fig. 5H-M). As described for the quantification of apoptotic nuclear fragments, most of the capillaries exposed to the control condition were not positive for active caspase-3 or presented very few positive hMVECs (Fig. 5H, I). The cytokine-exposed hMVECs networks presented a greater number of active caspase-3-positive capillaries (Fig. 5J, K) and even completely disorganized late apoptotic hMVECs structures (Fig. 5L). Quantification of the percentage of active caspase-3-positive CD31 segments revealed that 7.9% of CD31 segments were positive for active-caspase-3 in the control condition (Fig. 5M). This percentage increased to respectively 22.7% and 28.4% (non-significant) for the TNF only and IL-1β only conditions, and reached 70.2%, a 8.9 fold significant increase for the combined TNF/IL-1β condition.

After 3 days of exposure to cytokines, the secretion profiles of MMP-2 (Fig. 6A) and MMP-9 (Fig. 6B) were also examined using ELISA assays. Increased secreted levels were measured for both MMPs for all cytokine-treated conditions. MMP-2 was increased up to 5.0 fold for the combined TNF/IL-1β condition (Fig. 6A). MMP-9 secretion was strongly upregulated by TNF (up to 11 fold) in comparison to IL-1β alone (up to 3.2 fold) and TNF/IL-1β (up to 4.0 fold, Fig. 6B).

Discussion

TNF and IL-1β are potent pro-inflammatory cytokines that trigger many cell type-dependent biological processes. Evidences gathered from obesity-related studies provided important insights on the impact of pro-inflammatory cytokines on AT functions since adipose depots from obese individuals reveal a chronic low-grade inflammatory state.[53] In addition, TNF and IL-1β effects on ASC and adipocyte functions have been reported in the literature, mainly using various *in vitro* murine and human monolayer cultures or short-lived isolated adipocytes and explanted tissues,[23-32, 54] although an increasing number of studies are now using *in vivo* or *in vitro* 3D adipose models.[55-57]

Our 3D model incorporating hMVECs that form a stable network within engineered constructs featuring numerous adipocytes leads to a highly physiological human tissue considering the endogenous ECM elements produced by ASCs. Therefore, such hrATs recapitulate tissue responses in presence of inflammatory mediators by recreating a more integrated inflammatory microenvironment including direct cell contacts and ECM-signaling pathways. Fewer studies specifically describe the impact of inflammation on AT microvasculature[34-36] and contradictory effects have been reported when examining endothelial cells behavior in different experimental contexts.[37-44] We therefore submitted microvascularized AT substitutes (hrATs+hMVECs) to conditions mimicking chronic inflammation for up to 6 days.

First, we established the gene expression of TNF receptors (*TNFRSF1A*, *TNFRSF1B*) and IL-1β receptor signaling complex (*IL1R1*, *IL1RAP*) by the cells forming the reconstructed adipose sheets. Moreover, hMVEC gene expression for these receptors is consistent with other studies using *in vitro* cultured human microvascular endothelial cells shown to be responsive to TNF and IL-1β [58-60] and to express TNFR1 and TNFR2 [61] as well as IL1R1, IL1R2 and IL1RAP [62], both at the mRNA and the protein levels. This confirms that TNF and IL-1β can directly initiate signaling events and induce inflammation-responsive genes within the engineered constructs. At the histological level, the impact of cytokine treatments on hrATs+hMVECs was evidenced by increased tissue thickness, especially for the IL-1β stimulation. This is consistent with the suggested link between AT fibrosis and the infiltration of immune cells such as M1-type macrophages, which are major producers of TNF and IL-1β.[63]

The secretome of AT and ASCs is a very important feature in terms of their therapeutic potential in regenerative medicine.[64] Our results established the secretion by hrATs+hMVECs of the adipocyte-specific adiponectin as well as the ASC- and adipocyte-secreted proteins MCP-1, IL-6 and angiopoietin-1 for non-treated tissues, along with their modulation upon pro-inflammatory stimulation. More precisely, following exposure to each pro-inflammatory cytokine condition, the secretion of the anti-inflammatory factor adiponectin[8] was decreased in hrATs+hMVECs. This was also reported in a study using monolayer cultures of human *in vitro* differentiated adipocytes exposed to 10 ng ml^{-1} of TNF or IL-1β for 3 and 7 days.[28] In other studies, a small decrease in the secreted level of adiponectin was observed after a 24 h exposure of human *in vitro* differentiated adipocytes to 25 ng ml^{-1} of TNF,[32] while a more drastic decrease was observed for a 24 h incubation with 10 and 20 ng ml^{-1} of murine IL-1β.[29] Of note, decreased adiponectin plasma levels are observed for obese individuals[65] and a negative correlation between plasma adiponectin level and BMI has been established.[65, 66]

Following exposure to pro-inflammatory cytokines, increases in the secretion levels of MCP-1, IL-6 and Ang-1 were observed for hrATs+hMVECs in each cytokine condition. The inflammatory mediators MCP-1 and IL-6 are also reported to be increased for human *in vitro* differentiated or isolated adipocytes treated with 5-100 ng ml^{-1} TNF or 10 ng ml^{-1} IL-1β for 24 h or less.[30-32] For Ang-1, its gene expression was

reported to be increased in rheumatoid synovial tissue as well as in rheumatoid synovial fibroblast lines treated or not with 2 ng ml^{-1} TNF.[67] Finally, obesity is associated with increased plasma or serum concentrations of MCP-1, IL-6 and Ang-1.[68-70]

We next evaluated how the chronic pro-inflammatory microenvironment would impact the formed capillary network of hrATs+hMVECs over 6 days *in vitro* using confocal imaging of large surface areas. For the TNF/IL-1β combination, we observed a disorganization of the capillary network characterized by a reduction of the total network length and a lower percentage of branched structures. Given that the secretion of Ang-2 is predominantly from hMVECs, the reduced Ang-2 levels after 3 and 6 days of cytokine exposure to TNF and/or IL-1β are consistent with the smaller extent and disorganization of the network. Hutton and collaborators created fibrin gel spheroids containing human ASCs induced towards vascular morphogenesis.[71] A 48 h treatment with 100 ng ml^{-1} TNF decreased the CD31-positive vascular network length and number of junctions, while a 10 ng ml^{-1} treatment did not induce significant variations and a 0.1 ng ml^{-1} treatment favored vascularization.[71] In comparison, our results revealed that 10 ng ml^{-1} of TNF alone did not induce marked variations while the combination of TNF/IL-1β had the most drastic effect on the disorganization of the network. Of interest, during the 6-day incubation period, mock-treated hrATs+hMVECs featured a stable capillary network.

The binding of TNF and IL-1β to their receptors can induce the activation of different signaling pathways leading to the transcription of survival and inflammation-related genes.[72, 73] TNF and IL-1β have also been described to induce apoptosis in endothelial cells.[38-41] Indeed, these cells are important targets of inflammation[74] and endothelial cell apoptosis would play a role in vascular diseases such as atherosclerosis.[75] Condensed chromatin, nuclear fragmentation and caspase activation are apoptosis-related features used for vessel apoptosis detection.[76] In hrATs+hMVECs incubated with TNF/IL-1β, we observed increased Hoechst-positive condensed nuclear fragments and active caspase-3 presence within capillaries. These increased apoptotic markers point towards a contribution of endothelial cell death to the disorganization of the network. Additional inflammation-activated cellular processes such as oxidative stress and proteolytic events are also likely involved. MMP-2 and MMP-9 are secreted by human AT and have been reported to participate to vascular formation and remodeling.[16, 77] Following exposure of hrATs+hMVECs to the pro-inflammatory cytokines, increased secreted levels of MMP-2 and MMP-9 were detected for each condition, although TNF-induced MMP-9 secretion seemed to be downregulated by IL-1β. Consistent with our results, increased MMP-9 secretion and MMP-2 proteolytic activity have been noted in supernatants from human TNF-treated ASCs.[78] A similar downregulation of TNF-induced MMP-9 secretion by IL-1β was also observed for human kidney cells.[79] Taken together, these results suggest a contribution of MMP-mediated proteolytic events to the remodeling of hrATs+hMVECs matrix and capillary network.

Conclusions

ASCs are producers of endogenous ECM components acting as biomaterials and providing topographical and signaling cues appropriately recapitulating cellular functions. Using our ASC-based hrATs model, we determined that prolonged inflammation induces an important modulation of the tissues secretory profile and a disorganization of the preformed capillary network. Future studies evaluating the potency of preconditioning agents to dampen inflammatory responses will be of particular importance for the development of improved adipose substitutes for regenerative medicine applications.

Acknowledgements

This work was supported by Canadian Institutes of Health Research (CIHR) grants (#84368 and #111233). We acknowledge the support of the Centre de recherche du CHU de Québec, of the Fonds de recherche du Québec-Santé (FRQ-S) and of the Réseau ThéCell du FRQ-S. MP received studentships from National Science and Engineering Research Council of Canada (NSERC), FRQ-S and Canadian Federation of University Women (CFUW). MS received studentships from CIHR and Laval University Faculty of Medicine. KA obtained a Fonds de la recherche du Québec - Nature et technologies (FRQ-NT) studentship. JF received a FRQ-S Junior 2 career award. The confocal imaging system was obtained through the Fonds des leaders program from Canada Foundation for Innovation (CFI) to JF. The authors are grateful to V. Trottier and P. Morissette Martin for technical assistance and to S. Chabaud and V. Moulin for providing human skin microvascular endothelial cells. We also thank the Centre de recherche du CHU de Québec Gene Expression Platform for qRT-PCR analyses.

References

1. D. L. Crandall, G. J. Hausman and J. G. Kral, *Microcirculation*, 1997, **4**, 211-232.
2. P. A. Zuk, M. Zhu, H. Mizuno, J. Huang, J. W. Futrell, A. J. Katz, P. Benhaim, H. P. Lorenz and M. H. Hedrick, *Tissue Eng*, 2001, **7**, 211-228.
3. Y. Cao, *J Clin Invest*, 2007, **117**, 2362-2368.
4. E. E. Kershaw and J. S. Flier, *J Clin Endocrinol Metab*, 2004, **89**, 2548-2556.
5. J. B. Prins, *Best Pract Res Clin Endocrinol Metab*, 2002, **16**, 639-651.
6. H. Hauner, *Physiol Behav*, 2004, **83**, 653-658.
7. P. Trayhurn, *Acta Physiol Scand*, 2005, **184**, 285-293.
8. K. Robinson, J. Prins and B. Venkatesh, *Crit Care*, 2011, **15**, 221.
9. P. Trayhurn and I. S. Wood, *Br J Nutr*, 2004, **92**, 347-355.
10. J. N. Fain, *Vitam Horm*, 2006, **74**, 443-477.

11. G. Thurston, J. S. Rudge, E. Ioffe, H. Zhou, L. Ross, S. D. Croll, N. Glazer, J. Holash, D. M. McDonald and G. D. Yancopoulos, *Nat Med*, 2000, **6**, 460-463.
12. P. C. Maisonpierre, C. Suri, P. F. Jones, S. Bartunkova, S. J. Wiegand, C. Radziejewski, D. Compton, J. McClain, T. H. Aldrich, N. Papadopoulos, T. J. Daly, S. Davis, T. N. Sato and G. D. Yancopoulos, *Science*, 1997, **277**, 55-60.
13. S. M. Dallabrida, D. Zurakowski, S. C. Shih, L. E. Smith, J. Folkman, K. S. Moulton and M. A. Rupnick, *Biochem Biophys Res Commun*, 2003, **311**, 563-571.
14. V. W. van Hinsbergh and P. Koolwijk, *Cardiovasc Res*, 2008, **78**, 203-212.
15. Q. X. Sang, *Cell Res*, 1998, **8**, 171-177.
16. A. Bouloumie, C. Sengenes, G. Portolan, J. Galitzky and M. Lafontan, *Diabetes*, 2001, **50**, 2080-2086.
17. M. C. Tanzi and S. Fare, *Expert Rev Med Devices*, 2009, **6**, 533-551.
18. M. W. Laschke, Y. Harder, M. Amon, I. Martin, J. Farhadi, A. Ring, N. Torio-Padron, R. Schramm, M. Rucker, D. Junker, J. M. Haufel, C. Carvalho, M. Heberer, G. Germann, B. Vollmar and M. D. Menger, *Tissue Eng*, 2006, **12**, 2093-2104.
19. E. C. Novosel, C. Kleinhans and P. J. Kluger, *Adv Drug Deliv Rev*, 2011, **63**, 300-311.
20. M. W. Laschke and M. D. Menger, *Eur Surg Res*, 2012, **48**, 85-92.
21. A. Crupi, A. Costa, A. Tarnok, S. Melzer and L. Teodori, *Eur J Immunol*, 2015, **45**, 3222-3236.
22. D. B. Hom, *Otolaryngol Clin North Am*, 1994, **27**, 13-24.
23. T. Petruschke and H. Hauner, *J Clin Endocrinol Metab*, 1993, **76**, 742-747.
24. H. Xing, J. P. Northrop, J. R. Grove, K. E. Kilpatrick, J. L. Su and G. M. Ringold, *Endocrinology*, 1997, **138**, 2776-2783.
25. J. Ohsumi, S. Sakakibara, J. Yamaguchi, K. Miyadai, S. Yoshioka, T. Fujiwara, H. Horikoshi and N. Serizawa, *Endocrinology*, 1994, **135**, 2279-2282.
26. M. Ryden, E. Arvidsson, L. Blomqvist, L. Perbeck, A. Dicker and P. Arner, *Biochem Biophys Res Commun*, 2004, **318**, 168-175.
27. I. Hardardottir, W. Doerrler, K. R. Feingold and C. Grunfeld, *Biochem Biophys Res Commun*, 1992, **186**, 237-243.
28. P. J. Simons, P. S. van den Pangaart, J. M. Aerts and L. Boon, *J Endocrinol*, 2007, **192**, 289-299.
29. C. Lagathu, L. Yvan-Charvet, J. P. Bastard, M. Maachi, A. Quignard-Boulange, J. Capeau and M. Caron, *Diabetologia*, 2006, **49**, 2162-2173.
30. L. Flower, R. Gray, J. Pinkney and V. Mohamed-Ali, *Cytokine*, 2003, **21**, 32-37.
31. B. Wang, J. R. Jenkins and P. Trayhurn, *Am J Physiol Endocrinol Metab*, 2005, **288**, E731-740.
32. B. Wang and P. Trayhurn, *Pflugers Arch*, 2006, **452**, 418-427.
33. K. Aubin, M. Safoine, M. Proulx, M. A. Audet-Casgrain, J. F. Cote, F. A. Tetu, A. Roy and J. Fradette, *PLoS One*, 2015, **10**, e0137612.
34. G. Singer and D. N. Granger, *Microcirculation*, 2007, **14**, 375-387.
35. J. Ye, *Curr Diab Rep*, 2011, **11**, 203-210.
36. N. Sato, H. Nariuchi, N. Tsuruoka, T. Nishihara, J. G. Beitz, P. Calabresi and A. R. Frackelton, Jr., *J Invest Dermatol*, 1990, **95**, 85S-89S.
37. D. J. Mountain, M. Singh and K. Singh, *Life Sci*, 2008, **82**, 1224-1230.
38. S. S. Deshpande, P. Angkeow, J. Huang, M. Ozaki and K. Irani, *FASEB J*, 2000, **14**, 1705-1714.
39. B. Robaye, R. Mosselmans, W. Fiers, J. E. Dumont and P. Galand, *Am J Pathol*, 1991, **138**, 447-453.
40. A. Karsan, E. Yee and J. M. Harlan, *J Biol Chem*, 1996, **271**, 27201-27204.
41. D. Wang, Q. Wang, G. Yan, Y. Qiao, L. Sun, B. Zhu, C. Tang and Y. Gu, *Biochem Biophys Res Commun*, 2015, **466**, 607-614.
42. S. Yoshida, M. Ono, T. Shono, H. Izumi, T. Ishibashi, H. Suzuki and M. Kuwano, *Mol Cell Biol*, 1997, **17**, 4015-4023.
43. S. J. Leibovich, P. J. Polverini, H. M. Shepard, D. M. Wiseman, V. Shively and N. Nuseir, *Nature*, 1987, **329**, 630-632.
44. F. Fan, O. Stoeltzing, W. Liu, M. F. McCarty, Y. D. Jung, N. Reinmuth and L. M. Ellis, *Cancer Res*, 2004, **64**, 3186-3190.
45. K. Aubin, C. Vincent, M. Proulx, D. Mayrand and J. Fradette, *Acta Biomater*, 2015, **11**, 333-345.
46. M. Vermette, V. Trottier, V. Menard, L. Saint-Pierre, A. Roy and J. Fradette, *Biomaterials*, 2007, **28**, 2850-2860.
47. B. Labbe, G. Marceau-Fortier and J. Fradette, *Methods Mol Biol*, 2011, **702**, 429-441.
48. K. R. Feingold, W. Doerrler, C. A. Dinarello, W. Fiers and C. Grunfeld, *Endocrinology*, 1992, **130**, 10-16.
49. V. Luu-The, N. Paquet, E. Calvo and J. Cumps, *Biotechniques*, 2005, **38**, 287-293.
50. S. A. Bustin, V. Benes, J. A. Garson, J. Hellemans, J. Huggett, M. Kubista, R. Mueller, T. Nolan, M. W. Pfaffl, G. L. Shipley, J. Vandesompele and C. T. Wittwer, *Clin Chem*, 2009, **55**, 611-622.
51. S. A. Bustin, J. F. Beaulieu, J. Huggett, R. Jaggi, F. S. Kibenge, P. A. Olsvik, L. C. Penning and S. Toegel, *BMC Mol Biol*, 2010, **11**, 74.
52. D. Mayrand and J. Fradette, in *Methods in Molecular Biology*, eds. J. M. Gimble and B. A. Bunnell, Springer, in press.
53. M. F. Gregor and G. S. Hotamisligil, *Annu Rev Immunol*, 2011, **29**, 415-445.
54. J. M. Bruun, S. B. Pedersen, K. Kristensen and B. Richelsen, *Mol Cell Endocrinol*, 2002, **190**, 91-99.
55. P. A. Turner, Y. Tang, S. J. Weiss and A. V. Janorkar, *Tissue Eng Part A*, 2015, **21**, 1837-1847.
56. H. E. Lilja, W. A. Morrison, X. L. Han, J. Palmer, C. Taylor, R. Tee, A. Moller, E. W. Thompson and K. M. Abberton, *Stem Cells Dev*, 2013, **22**, 1602-1613.
57. V. Pellegrinelli, C. Rouault, N. Veyrie, K. Clement and D. Lacasa, *Diabetes*, 2014, **63**, 535-549.
58. M. Detmar, S. Tenorio, U. Hettmannsperger, Z. Ruszczak and C. E. Orfanos, *J Invest Dermatol*, 1992, **98**, 147-153.
59. L. I. Romero, D. N. Zhang, G. S. Herron and M. A. Karasek, *J Cell Physiol*, 1997, **173**, 84-92.
60. R. A. Swerlick, K. H. Lee, L. J. Li, N. T. Sepp, S. W. Caughman and T. J. Lawley, *J Immunol*, 1992, **149**, 698-705.
61. B. Ding, N. C. Kirkiles-Smith and J. S. Pober, *J Biol Chem*, 2009, **284**, 19331-19339.
62. A. Bourdiec, D. Bedard, C. V. Rao and A. Akoum, *Am J Reprod Immunol*, 2013, **70**, 127-138.

63. C. Buechler, S. Krautbauer and K. Eisinger, *World J Diabetes*, 2015, **6**, 548-553.
64. A. J. Salgado, R. L. Reis, N. J. Sousa and J. M. Gimble, *Curr Stem Cell Res Ther*, 2010, **5**, 103-110.
65. Y. Arita, S. Kihara, N. Ouchi, M. Takahashi, K. Maeda, J. Miyagawa, K. Hotta, I. Shimomura, T. Nakamura, K. Miyaoka, H. Kuriyama, M. Nishida, S. Yamashita, K. Okubo, K. Matsubara, M. Muraguchi, Y. Ohmoto, T. Funahashi and Y. Matsuzawa, *Biochem Biophys Res Commun*, 1999, **257**, 79-83.
66. C. Weyer, T. Funahashi, S. Tanaka, K. Hotta, Y. Matsuzawa, R. E. Pratley and P. A. Tataranni, *J Clin Endocrinol Metab*, 2001, **86**, 1930-1935.
67. B. B. Scott, P. F. Zaratin, A. Colombo, M. J. Hansbury, J. D. Winkler and J. R. Jackson, *J Rheumatol*, 2002, **29**, 230-239.
68. J. M. Bruun, C. Verdich, S. Toubro, A. Astrup and B. Richelsen, *Eur J Endocrinol*, 2003, **148**, 535-542.
69. V. Catalan, J. Gomez-Ambrosi, B. Ramirez, F. Rotellar, C. Pastor, C. Silva, A. Rodriguez, M. J. Gil, J. A. Cienfuegos and G. Fruhbeck, *Obes Surg*, 2007, **17**, 1464-1474.
70. K. B. Cullberg, T. Christiansen, S. K. Paulsen, J. M. Bruun, S. B. Pedersen and B. Richelsen, *Obesity (Silver Spring)*, 2013, **21**, 454-460.
71. D. L. Hutton, R. Kondragunta, E. M. Moore, B. P. Hung, X. Jia and W. L. Grayson, *PLoS One*, 2014, **9**, e107199.
72. M. S. Hayden and S. Ghosh, *Semin Immunol*, 2014, **26**, 253-266.
73. A. Weber, P. Wasiliew and M. Kracht, *Sci Signal*, 2010, **3**, cm1.
74. L. A. Madge and J. S. Pober, *Exp Mol Pathol*, 2001, **70**, 317-325.
75. J. C. Choy, D. J. Granville, D. W. Hunt and B. M. McManus, *J Mol Cell Cardiol*, 2001, **33**, 1673-1690.
76. W. A. Boivin and D. J. Granville, *Methods Mol Med*, 2007, **139**, 181-195.
77. Q. Chen, M. Jin, F. Yang, J. Zhu, Q. Xiao and L. Zhang, *Mediators Inflamm*, 2013, **2013**, 928315.
78. E. S. Zubkova, I. B. Beloglazova, P. I. Makarevich, M. A. Boldyreva, O. Y. Sukhareva, M. V. Shestakova, K. V. Dergilev, Y. V. Parfyonova and M. Y. Menshikov, *J Cell Biochem*, 2016, **117**, 180-196.
79. L. E. Nee, T. McMorrow, E. Campbell, C. Slattery and M. P. Ryan, *Kidney Int*, 2004, **66**, 1376-1386.

Journal of Materials Chemistry B

ARTICLE

Figures

Fig. 1

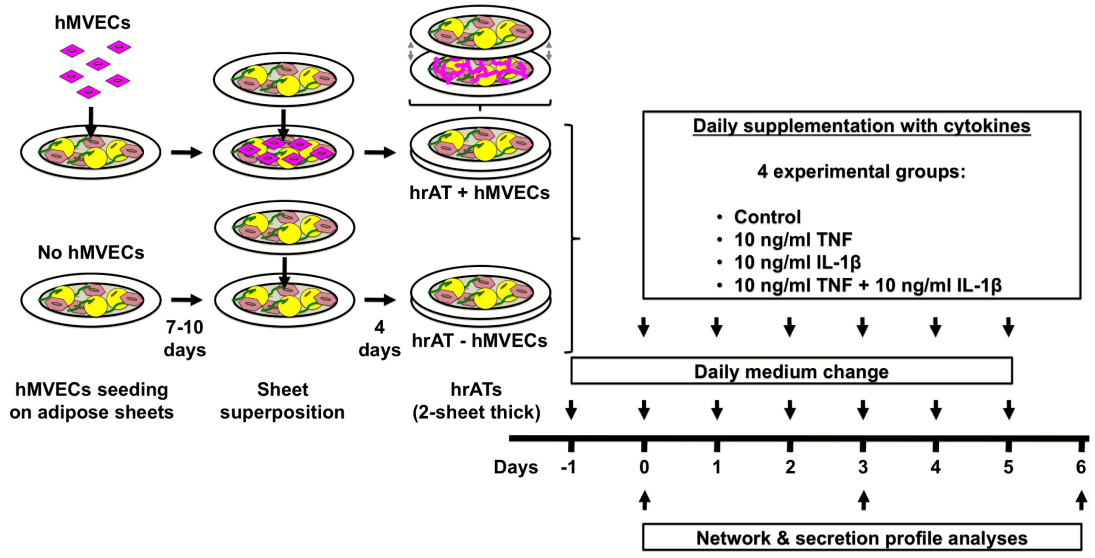

Fig. 1 Schematic representation of the experimental design for hrATs production and *in vitro* pro-inflammatory cytokine treatments. Subgroups of human reconstructed adipose sheets were seeded or not with hMVECs and maintained in culture for 7-10 days before their superposition to produce either hrATs+hMVECs or their counterparts devoid of endothelial cells (hrATs-hMVECs). Both tissue types were cultured for an additional 5 days to allow cohesion between cell sheets and favor capillary network formation and remodeling. At day 0 of treatment (day 33-41 of culture), 10 ng ml^{-1} TNF, 10 ng ml^{-1} IL-1β or the combination of both was added daily to the cultures during medium change. The impact of cytokines on the secretion profile and the capillary-like network organization were studied at day 0, 3, and 6 of treatment in comparison to control tissues.

Fig. 2

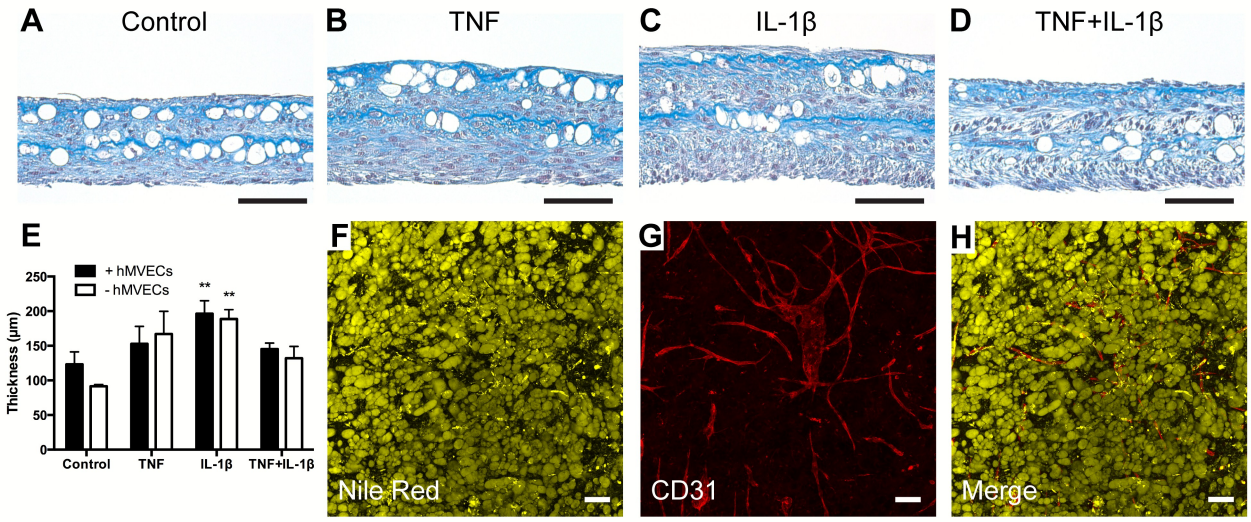

Fig. 2 Characterization of hrATs. A-D) Histological aspect of hrATs+hMVECs following Masson's trichrome staining of tissue transverse sections and E) quantification of tissue thickness after 6 days of cytokine exposure. F-H) Confocal images of control tissues showing F) Nile Red staining of intracellular lipids within adipocytes, which are abundant in hrATs, and G) CD31-expressing endothelial cells revealing a stable capillary network (day 6, untreated group). H) Merged images of F and G). F, H) A signal from the Vybrant Dil staining used for hMVECs tracking is also detected in the channel used for Nile Red imaging. Bars: 100 µm.

Fig. 3

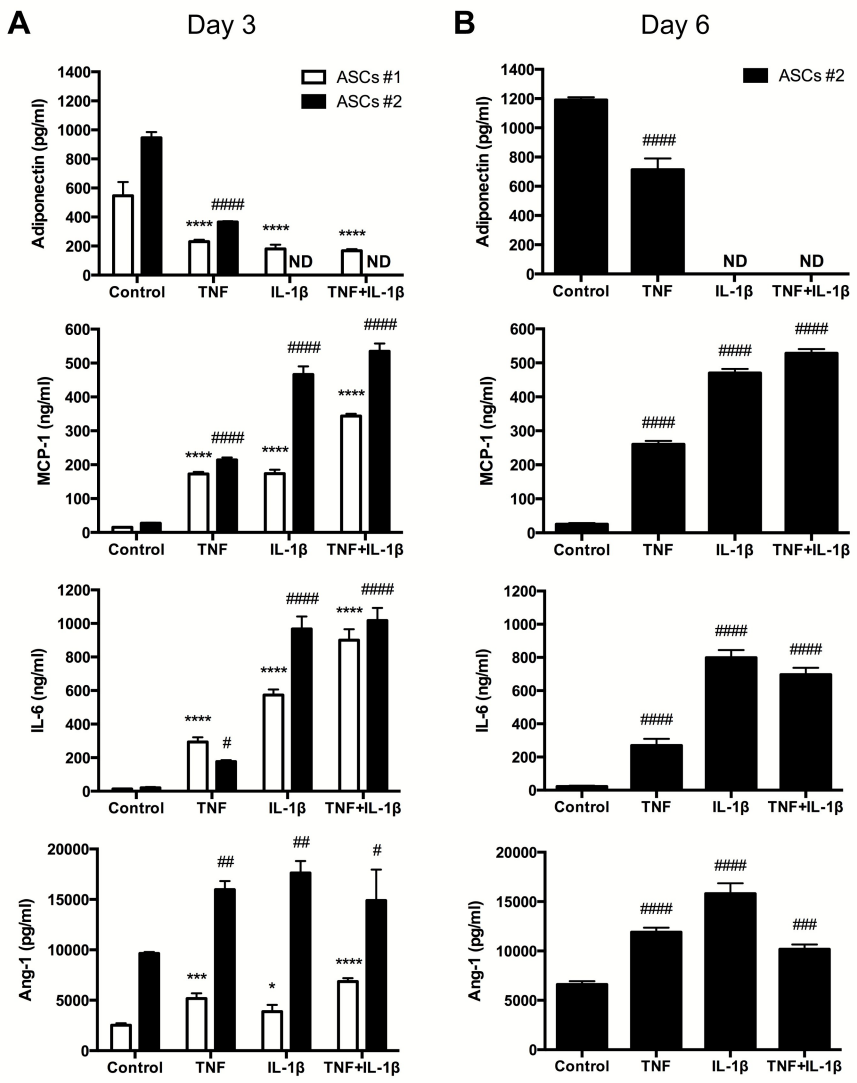

Fig. 3 Impact of pro-inflammatory cytokines on the secretory profile of cells within hrATs+hMVECs. Secretion levels of adiponectin, MCP-1, IL-6 and Ang-1 after A) 3 and B) 6 days of treatment. ND: Not detected.

Fig. 4

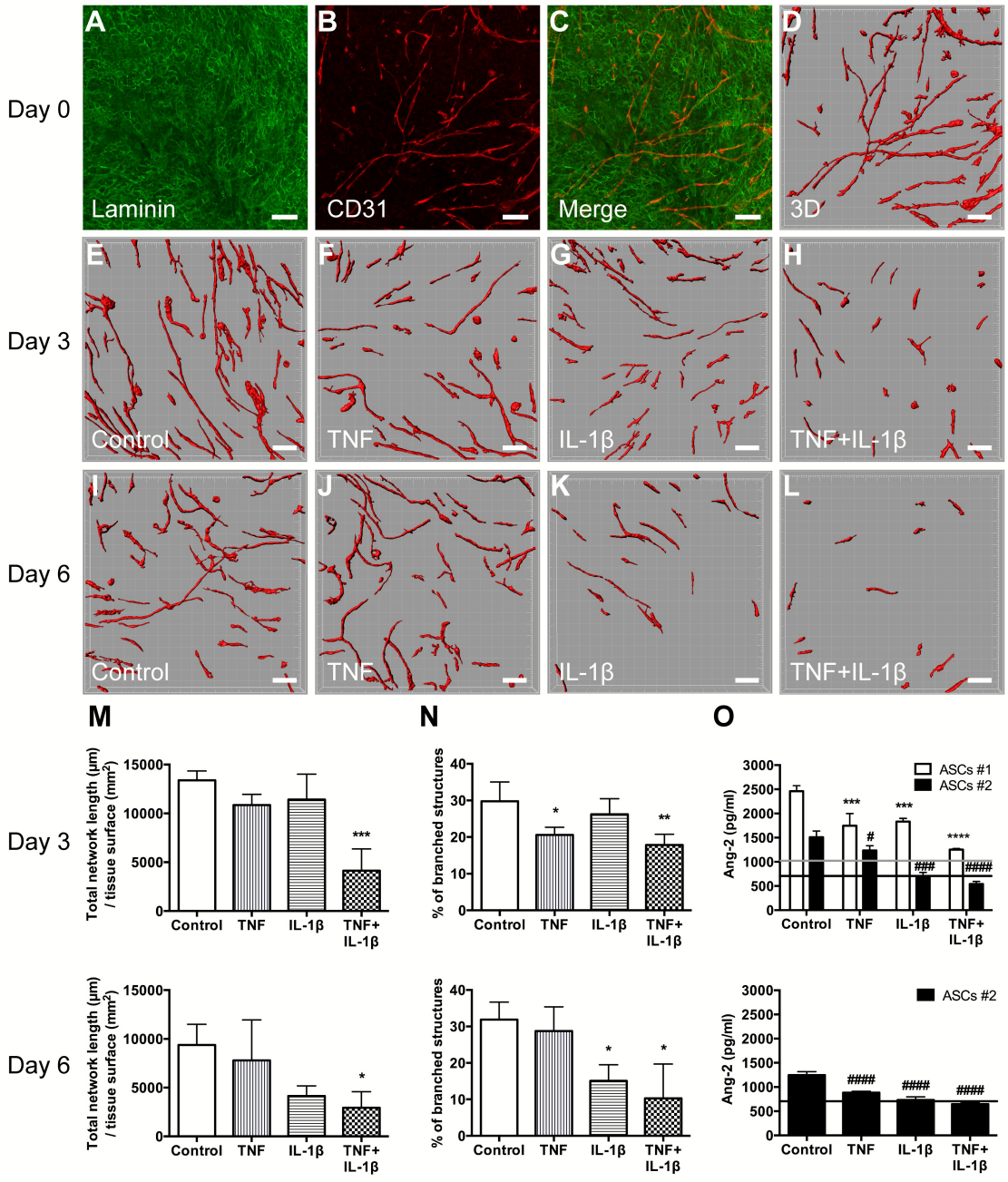

Fig. 4 Impact of pro-inflammatory cytokines on the capillary network of hrATs+hMVECs. Confocal images of hrATs+hMVECs before cytokine treatment reveal A) an abundant laminin expression and B) an extensive array of CD31-positive capillary-like structures. C) Merged images of A and B). D) 3D isosurface reconstruction of the CD31-positive capillary network shown in B). E-L) 3D isosurface reconstructions of the capillary networks showing the impact of pro-inflammatory cytokines after 3 and 6 days of incubation. M) Quantification of the total length of the capillary network per mm^2 of tissue and N) quantification of the percentage of branched capillary structures after 3 and 6 days of treatment. O) Impact of pro-inflammatory cytokines on the Ang-2 secretion profile at both time-points. Horizontal lines indicate the levels of Ang-2 detected in the control cell-free medium (gray line, ASCs #1; black line, ASCs #2). Bars: 100 µm.

Fig. 5

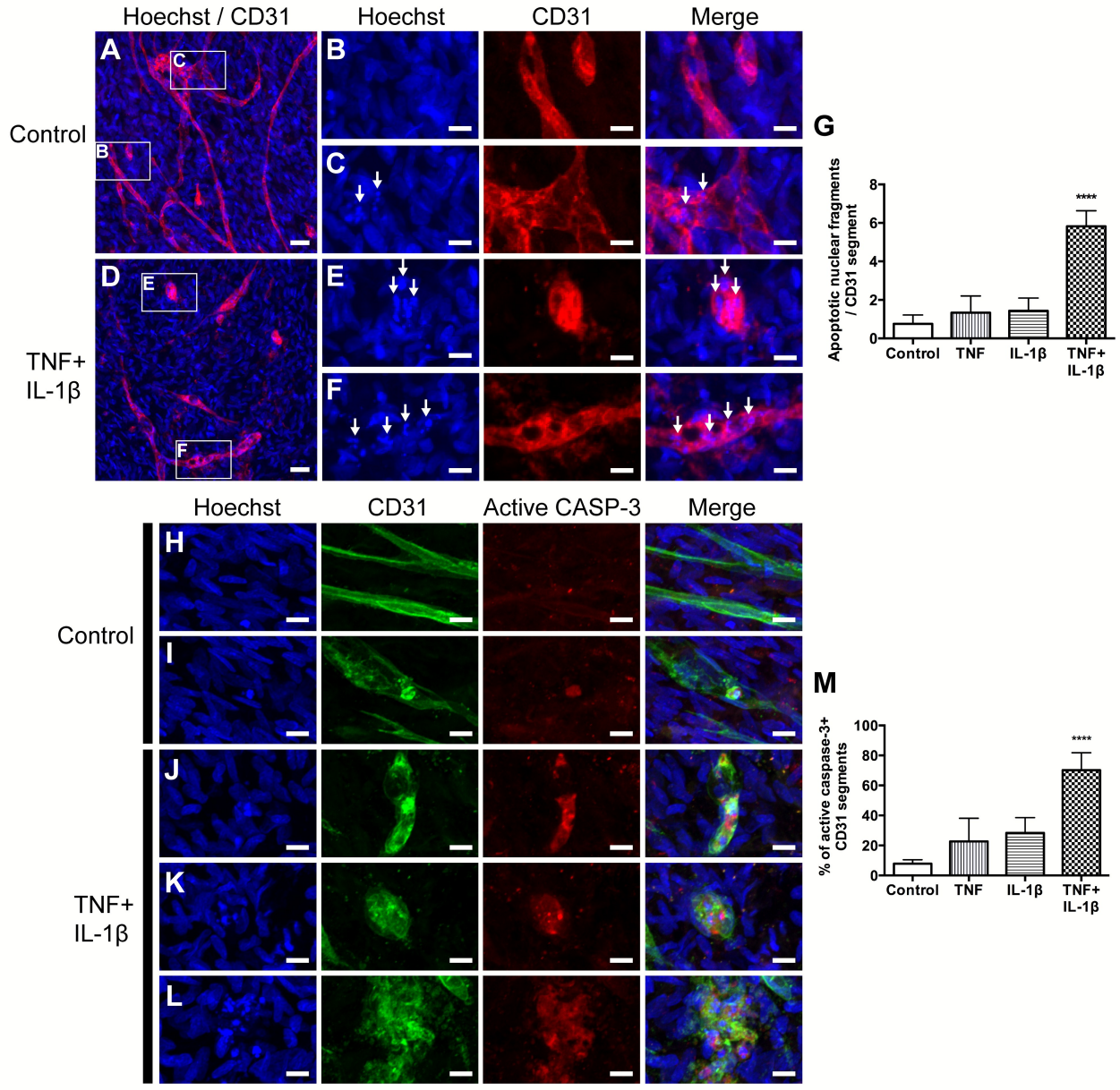

Fig. 5 Detection of apoptotic cells within the capillary network of hrATs+hMVECs after 3 days of incubation with pro-inflammatory cytokines. A-F) Confocal images showing Hoechst 33258 and CD31 staining. B, C) Magnified views of boxed regions shown in A). E, F) Images magnified from the boxed regions shown in D). G) Quantification of apoptotic nuclear fragments per CD31-expressing capillary segment. H-L) Confocal images showing Hoechst 33258, CD31 and active caspase-3 labelings. M) Quantification of the percentage of active caspase-3-positive CD31 segments. Bars: A, D 25 µm; B, C, E, F, H-L 10 µm. Arrows indicate Hoechst-positive condensed nuclear fragments.

Fig. 6

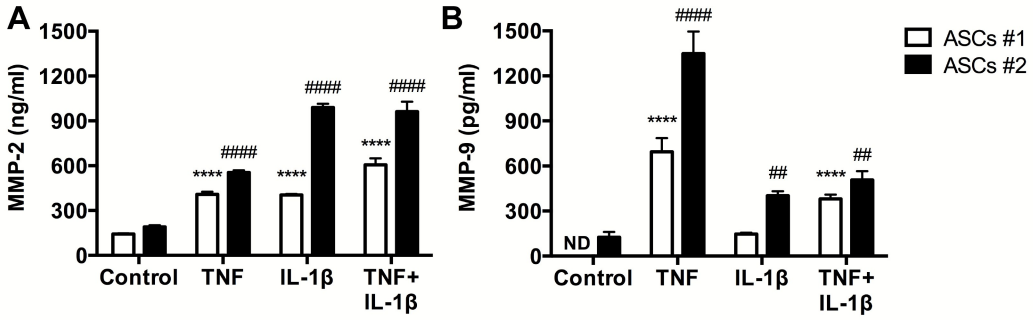

Fig. 6 Impact of pro-inflammatory cytokines on A) MMP-2 and B) MMP-9 secretion from hrATs+hMVECs after 3 days of cytokine exposure. ND: Not detected.

Table of contents

Inflammatory cytokines lead to capillary network disorganization and secreted factors modulation within human microvascularized engineered adipose tissues.